Natural Hazards and Earth System Sciences

Open Access

Automated classification of Persistent Scatterers Interferometry time series

M. Berti[1], A. Corsini[2], S. Franceschini[1], and J. P. Iannacone[2]

[1]Dipartimento di Scienze Biologiche, Geologiche e Ambientali, Università di Bologna – Via Zamboni 67, 40127 Bologna, Italy
[2]Dipartimento di Scienze Chimiche e Geologiche, Università di Modena e Reggio Emilia – Largo S. Eufemia 19, 41121 Modena, Italy

Correspondence to: M. Berti (matteo.berti@unibo.it)

Abstract. We present a new method for the automatic classification of Persistent Scatters Interferometry (PSI) time series based on a conditional sequence of statistical tests. Time series are classified into distinctive predefined target trends, such as uncorrelated, linear, quadratic, bilinear and discontinuous, that describe different styles of ground deformation. Our automatic analysis overcomes limits related to the visual classification of PSI time series, which cannot be carried out systematically for large datasets. The method has been tested with reference to landslides using PSI datasets covering the northern Apennines of Italy. The clear distinction between the relative frequency of uncorrelated, linear and non-linear time series with respect to mean velocity distribution suggests that different target trends are related to different physical processes that are likely to control slope movements. The spatial distribution of classified time series is also consistent with respect the known distribution of flat areas, slopes and landslides in the tests area. Classified time series enhances the radar interpretation of slope movements at the site scale, pointing out significant advantages in comparison with the conventional analysis based solely on the mean velocity. The test application also warns against potentially misleading classification outputs in case of datasets affected by systematic errors. Although the method was developed and tested to investigate landslides, it should be also useful for the analysis of other ground deformation processes such as subsidence, swelling/shrinkage of soils, or uplifts due to deep injections in reservoirs.

1 Introduction

The detection of ground displacements by space borne synthetic aperture radar interferometry has progressed, over the last two decades, from the use of single interferograms, as in the pioneer work of Massonnet and Feigl (1998), to the use of advanced persistent scatterers multi-interferometry (PSI) techniques, such as Permanent Scatterers (PS), Small Baseline Subset (SBAS), Interferometric Point Target Analysis (IPTA), Persistent Scatterers Pairs (PSP) (Ferretti et al., 2001; Berardino et al., 2002; Werner et al., 2003; Costantini et al., 2008). The success of PSI techniques is due to the ever increasing availability of space borne radar data (which nowadays cover most of the globe with repeat pass ranging from days to months) and to the fact that results are provided as spatially georeferenced datasets which can be directly integrated in GIS with other available topographic, photographic and geologic ancillary data.

In landslide studies, interferometry has been considered as a powerful tool for hazard management (Corsini et al., 2006) and the term "radar interpretation" has been introduced to indicate the use of PSI datasets to map and characterize slope dynamics in conjunction to ground truths survey (Farina et al., 2008). However, such analyses have been so far carried out by only considering the mean displacement rate over the monitoring period (e.g. Righini et al., 2012). PSI time series, in fact, are somewhat noisy and difficult to interpret because of the detrimental effect of residual atmospheric errors and by problems related to phase aliasing. For these reasons a linear regression model is generally fitted to data and the average displacement rate is used to describe the entire time series.

On the other hand, several studies have shown that even the analysis of a few relevant time series may provide useful information on slope dynamics (Meisina et al., 2008; Cigna et al., 2011). Cigna et al. (2011), in particular, manually classify the time series of several radar targets to identify the change in deformation rate caused by tectonically induced land motions. More recently, Cigna et al. (2012) further extended their analysis and developed a semi-automatic method to characterize the change in velocity within a PS time series. The novelty of the method lies in the definition of two statistical indexes capable of describing quantitatively the variation of the displacement rate, thus improving the current methods of radar interpretation. Their approach, however, still requires a preliminary, visual analysis of the time series to locate the breakpoint at which the change in motion occurs. Any supervised manual classification of time series is a tedious, time-consuming and subjective work which cannot be carried out for large datasets. Hence, criteria and methods for an objective, automated classification of time series included in large datasets are needed for enhancing radar interpretation capabilities at the regional scale and for providing, at a glance, a comprehensive picture of the evolution of slope movements over the period covered by the interferometric analysis.

The goal of this work is to present a procedure based on a sequence of statistical characterization tests which allows one to automatically classify PSI time series into distinctive target trends and to retrieve, for each specific time series, descriptive parameters which can be used to characterize the magnitude and timing of changes in ground motion. To our best knowledge, one of the very few published attempts to propose a PSI time series clustering approach is that of Milone and Scepi (2011). They used the partition-based clustering algorithms CLARA (Clustering for Large Applications) which defines "k" clusters in an entire dataset on the basis of the identification of "k" representative objects in a sub-dataset. The type and the number of clusters are therefore specifically dependant on the dataset itself; if a different dataset is processed, different clusters are possibly generated. This is a relevant problem in radar interpretation since PSI information from different orbits, tracks and satellites datasets have usually to be used and compared. Our approach aims to overcome such a limitation, by allowing PSI time series to be clustered into fixed predefined target trends (uncorrelated, linear, quadratic, bilinear, discontinuous) which can be potentially recognized in any PSI dataset and that are believed to be interpretable in terms of physical processes related to slope instability. Inevitably, time series classification is affected by the quality of the dataset. In this paper, the proposed automated classification algorithm (hereafter referred to as PS-Time) has been tested with reference to landslides in the northern Apennines of Italy by using ENVISAT datasets available in the frame of EPRS-E project (Extraordinary Plan of Remote Sensing of the Environment) of the Italian Ministry of Environment. Datasets of the EPRS-E have been generated using standard PSI processing and are notoriously affected by a high noise-to-signal ratio. Nevertheless, results obtained with PS-Time show that even with such rough quality datasets, the method can provide results that are generally consistent with the nature of the analysed landslide phenomena and that, as such, can potentially improve radar interpretation of mass movements at regional to site-specific scale.

Throughout the paper, when we refer to "PSI data" or "PSI time series" we always refer to post-processed satellite data provided by the manufacturer. Issues related to data generation (atmospheric correction, use of suitable deformation models, unwrapping techniques) are not considered in the present analysis.

2 Methods

2.1 Identification of distinctive target trends in PSI time series

As the main goal of the research is to develop an automatic procedure that classifies the PSI time series according to their peculiar trends, the a priori identification of trends that might indicate changes in time of physical processes related to slope instability (or other terrain movements) is crucial in order to tailor the selection of suitable statistical techniques.

To this purpose we randomly selected 1000 time series from our sample dataset (see Sect. 3) and performed a visual analysis to find distinct patterns of displacement. Six recurrent patterns were observed and consequently identified as target trends in PSI time series (Fig. 1):

- Type 0: uncorrelated – displacement varies erratically in time.

- Type 1: linear – displacement increases linearly in time with constant velocity.

- Type 2 – quadratic: velocity varies continuously in time.

- Type 3 – bilinear: time series is segmented in two linear tracts of different velocity separated by a breakpoint in which the function is continuous.

- Type 4 – discontinuous with constant velocity: time series is segmented in two linear tracts of similar velocity separated by a breakpoint in which the function is discontinuous.

- Type 5 – discontinuous with variable velocity: time series is segmented in two linear tracts of different velocity separated by a breakpoint in which the function is discontinuous.

Uncorrelated time series (type 0) denote random fluctuations of displacements around zero and typically indicate stable PS (no significant movements during the monitoring period).
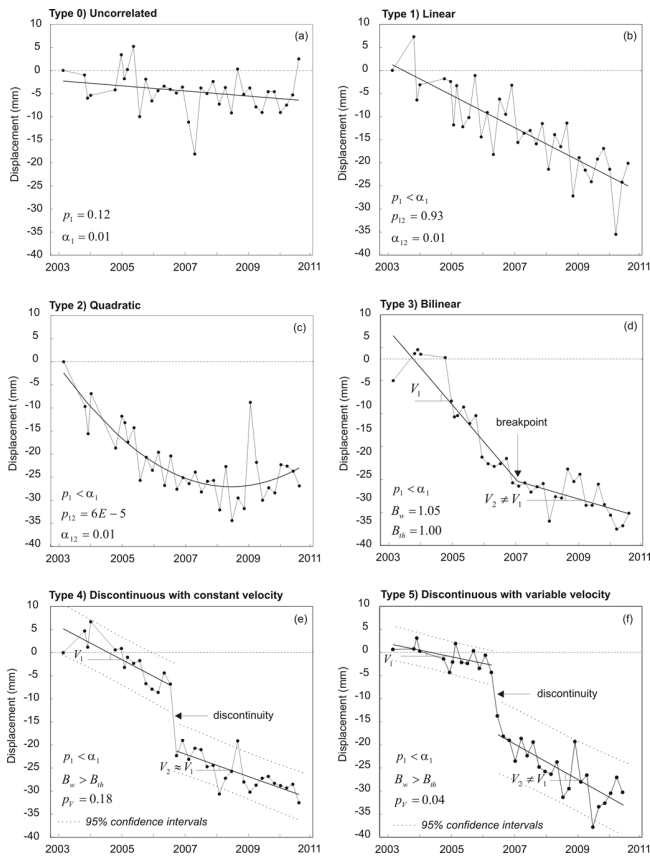
Fig. 1. Typical ground displacement trends identified by visual inspection of 1000 Permanent Scatterers time series. Letters indicate the results of the automatic classification obtained by statistical analyses (see text and Fig. 2).

Fig. 2. Workflow of the proposed method for the automatic classification of PSI time series.

Linear trends (type 1) denote ground displacements at constant rate and characterize ground deformation processes acting over long timescales (creep, natural subsidence, steady motion of dormant landslides). Non-linear trends (type 2 to 5) indicate a change of the displacement rate during the monitoring period. Regardless of whether this change is progressive (type 2), abrupt (type 3), or discontinuous (type 4–5), non-linear trends catch our attention because they indicate a variation of the displacement field. Types 0 and 1 correspond to the stable (S) and linear (L) "unaffected targets" proposed by Cigna et al. (2011); types 4 and 5 to their temporary (T) and permanent (P) "affected targets".

2.2 Statistical tests for automated classification of PSI time series

An automatic procedure based on the sequential application of a number of statistical tests (Fig. 2) was developed to classify each time series into one of the six target trends shown in Fig. 1. Each testing method is hereafter briefly described.
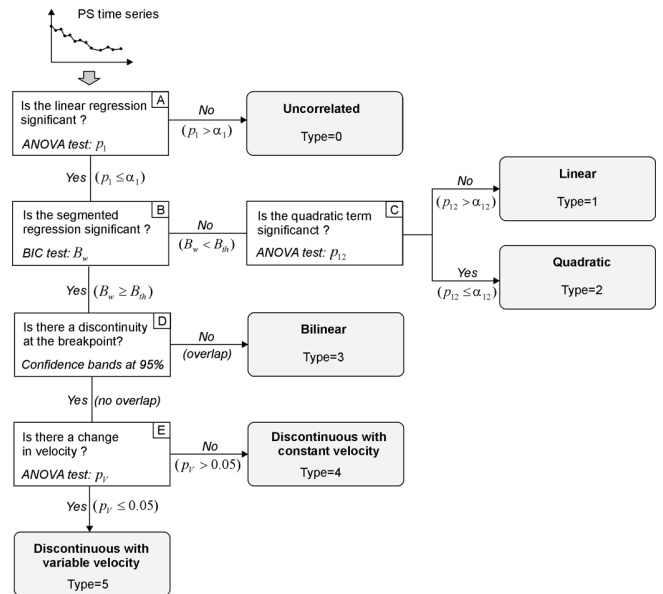
2.2.1 (A) linear regression

The first step in the analysis (test A in Fig. 2) is an ANOVA F test for the significance of the linear regression (Davis, 1986). The PS displacements are plotted against time and fitted by a linear regression model. The F statistic is then used to compute the probability value p_1 that the regression coefficient β_1 (the slope of the regression line) is equal to zero: if p_1 is less than the selected level of significance α_1, the null hypothesis of no correlation ($H_0 : \beta_1 = 0$) is rejected and we accept that there is a significant linear relationship between the two variables; conversely, if $p_1 > \alpha_1$ the null hypothesis cannot be rejected and we conclude that the two variables are not linearly correlated.

Obviously, the absence of a linear correlation does not imply that the displacements are randomly distributed with time because the time series could be described by a higher order model (Draper and Smith, 1981; Sen and Srivastava, 1990). Based on our experience, however, a time series with an average slope close to zero ($\beta_1 \approx 0$) typically indicates a stable PS with no appreciable movements. Therefore, if the linearity test fails ($p_1 > \alpha_1$) the time series is directly classified as "uncorrelated" (type = 0; Fig. 2)

2.2.2 (B) segmented regression

If linear regression is significant ($p_1 \leq \alpha_1$) the time series is tested against a bilinear model (test B, Fig. 2). The segmented regression, also known as piecewise or changepoint regression, is a regression technique in which the independent variable is divided into intervals and a separate line segment is used to fit each interval (Main et al., 1999; Steven, 2001). The

segments are introduced to see if there is an abrupt change in slope in the data and to determine where the change occurs (breakpoint).

For this analysis we follow the method proposed by Main et al. (1999):

1. The time series $t_1, \ldots, t_n$ is divided into two parts separated by a breakpoint t_b, which is moved along the series from $b = 5$ to $b = n - 5$ (we assume that a minimum of 5 data points is required to define a segment, in order to avoid very short segments at the beginning or at the end of the time series).

2. For each breakpoint, a two-line unconstrained model is fitted for the segments $t_1, \ldots, t_b$ and $t_{b+1}, \ldots, t_n$ and the goodness of fit is evaluated using the Bayesian Information Criterion BIC (Main et al., 1999):

$$\mathrm{BIC}(t_b) = \ln\left(\frac{\mathrm{RSS}}{n}\right) + \frac{(k+1)}{n}\ln(n), \qquad (1)$$

where RSS is the residual sum of squares and k is the number of parameters in the model ($k = 3$ for a two-line regression).

3. An overall linear and quadratic fit is computed for the entire series $t_1, \ldots, t_n$, and the corresponding values BIC_L and BIC_Q are computed by Eq. (1) using $k = 1$ for the linear model and $k = 2$ for a quadratic model.

The BIC criterion (Schwarz, 1978) is widely used in statistics for model identification and selection. It compares the performance of different models introducing a penalty term for the number of parameters in the model (the second term in Eq. 1). In this way the BIC resolves the problem of over-fitting and identifies the best model as the one that strike a balance between fitting the data well (low RSS) using only a few parameters (low k). As an example, Fig. 3 shows the values of $\mathrm{BIC}(t_b)$, BIC_L and BIC_Q computed for the time series shown in Fig. 1d.

By comparing the BIC values we infer cases where a double-slope assumption is statistically better than a linear or quadratic model. Specifically, the time series justifies a breakpoint if the minimum value of BIC for the segmented model ($\mathrm{BIC}_{\min}$) is lower than both BIC_L and BIC_Q:

if $\mathrm{BIC}_{\min} < (\mathrm{BIC}_L \text{ and } \mathrm{BIC}_Q)$

$\Rightarrow$ significant breakpoint exists in the time series. (2)

In the example of Fig. 3 the segmented regression outperforms both the quadratic and the linear fit. There is then statistical evidence of a breakpoint at the beginning of 2006 (compare Fig. 3 with Fig. 1d).

Although condition (2) suffices to establish the existence of a breakpoint, we used a more restrictive criterion that also allows the user to calibrate the test outcome. The breakpoint
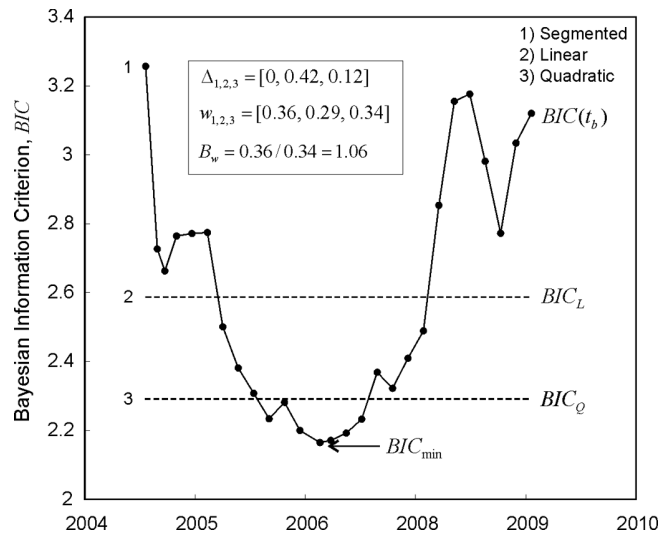

Fig. 3. Sample application of the segmented regression model to the time series shown in Fig. 1d. $\mathrm{BIC}(t_b)$ indicates the goodness of fit of the segmented model (lower values indicate better fit), computed by Eq. (1) as a function of the breakpoint position t_b. BIC_L and BIC_Q indicate the linear and quadratic fit computed for the entire time series. The inset shows the "evidence ratio" of the breakpoint computed by Eqs. (4) and (5).

is considered significant when the so-called "evidence ratio" B_w of the breakpoint exceeds a predefined threshold B_{th} (with $B_{th} \geq 1$), i.e.

if $B_w < B_{th} \Rightarrow$ no significant breakpoint (go to test C) (3a)
if $B_w \geq B_{th} \Rightarrow$ significant breakpoint (go to test D). (3b)

The evidence ratio B_w is computed as proposed by Wagenmakers and Farrell (2004):

$$B_w = \frac{w_1}{\max(w_2, w_3)}, \qquad (4)$$

where $w_{1,2,3}$ indicate the weights of the segmented, linear and quadratic model respectively. The weights are obtained by the normalization of the relative likelihoods:

$$w_i = \frac{\exp(-0.5\Delta_i)}{\sum_{i=1}^{3}\exp(-0.5\Delta_i)}, \qquad (5)$$

where the subscript $i = 1,2,3$ indicates the regression model and Δ_i is the difference of BIC between the bilinear model and the other two ($\Delta_1 = 0$; $\Delta_2 = \mathrm{BIC}_L - \mathrm{BIC}_{\min}$; $\Delta_3 = \mathrm{BIC}_Q - \mathrm{BIC}_{\min}$). In the example of Fig. 3 the evidence ratio is $B_w = 1.06$. Whether or not this value is significant depends on the selected threshold B_{th}, thus the higher the value of B_{th}, the more restrictive is the test. Note that the limit value $B_w = 1$ indicates the same fit for the bilinear and the other models ($\mathrm{BIC}_{\min} = \mathrm{BIC}_Q$ or $\mathrm{BIC}_{\min} = \mathrm{BIC}_L$).

2.2.3   (C) quadratic regression

If the time series is linearly correlated (test A passed) and does not have a breakpoint (test B failed) a quadratic fit is performed to test for the significance of quadratic over linear fit (Davis, 1986). An ANOVA F test evaluates the probability p_{12} that the quadric term is not contributing to the regression. If $p_{12} \leq \alpha_{12}$ (the selected level of significance) the quadratic term is making a significant contribution to the regression and should be retained. The time series is therefore classified as "quadratic" (type = 2). On the contrary, if $p_{12} > \alpha_{12}$ the additional term is not contributing significantly to the regression and the time series is classified as "linear" (type = 1).

2.2.4   (D) discontinuity test

The time series characterized by a significant breakpoint (test B passed) are tested to evaluate if there is a vertical jump in the data. The discontinuity test is based on a simple comparison of the prediction intervals at the 95 % level of significance computed for the two linear segments before and after the breakpoint (Weisberg, 1985), as shown in the example of Fig. 1e. The prediction intervals provide the range of expected values at the breakpoint: if the two intervals overlap each other, the time series is said to be continuous and it is classified as "bilinear" (type = 3); conversely, if the two intervals do not overlap, the series is said to be discontinuous at the breakpoint (Fig. 1e) and the two segments are tested for the equality of slopes.

2.2.5   (E) equality of slopes

The F test for the equality of slopes (Quinn and Keough, 2002) is applied to a discontinuous time series (test D passed) to evaluate if there is a significant difference of velocity before and after the breakpoint. The null hypothesis is that the two segments have the same slope ($H_0 : V_1 = V_2$). If the computed probability p_V is greater than the selected level of significance (set to 0.05), the null hypothesis cannot be rejected and we conclude that the difference in velocity is not significant ($V_1 \approx V_2$). The time series is then classified as "discontinuous with constant velocity" (type = 4). If $p_V \leq 0.05$, the null hypothesis is rejected ($V_1 \neq V_2$) and the time series is classified as "discontinuous with different velocity" (type = 5). It must be noted that the test for equality of slopes is adversely affected by data scattering and may have not enough power to detect differences that do in fact exist. The result of the test must be then carefully evaluated.

2.3   Accuracy of the method

The statistical tests employed in the analysis provide objective results based on well-established mathematical methods. The outcome of the automatic classification procedure is therefore inherently accurate from a statistical standpoint. In some cases, however, the classification results may not agree with our feeling and might provide results that seem to be "inaccurate". For instance, the ANOVA test of a noisy time series can recognize as "statistically significant" a linear trend that we found unimportant or trivial; or it can indicate as "not significant" a weak linear trend that we believe is very important. The problem in these cases is not the accuracy of the statistical test but the selected level of significance, that must be adjusted according to the specific needs.

In hypothesis testing, the significance level α is the criterion used for rejecting the null hypothesis H_0 (Davis, 1986). The value α is always small because it represents the probability of a Type I error, that is the probability of rejecting H_0 when it is actually true. A typical value of α is 0.05, but the choice of any cutoff significance level is arbitrary. For instance, a stiffer standard $\alpha = 0.01$ can be adopted if a stronger evidence is needed to reject the null hypothesis.

PSI time series have a limited number of data points and are often quite noisy. Therefore, statistical tests need to be stringent in identifying any non-random component and we should use small values of α. Doing so, however, we will likely lose important information on any deterministic signal. For this reason the statistical thresholds used in the analysis must be carefully calibrated. A way to perform the calibration is to run the analysis using different values of the significance levels, and to compare the results with that obtained by an expert visual classification. The suitable significance levels are those providing the best correlation with the expert judgment. This technique has been used to calibrate α_1 (test A), α_{12} (test C) and B_{th} (test B) in our sample application (Sect. 3.2).

2.4   Annual periodicity of time series

Several time series are characterized by cyclic fluctuations of the displacement values over the monitoring period. The amplitude of these fluctuations appears to be quite variable in time, but the period is relatively constant, with a typical periodicity of about one year. Such a cyclic behavior is usually observed in slow-moving PS and tends to disappear when the velocity increase. In most cases, periodic time series are classified as "uncorrelated" (type = 0) because the linear velocity is close to zero.

The detection of periodic time series can be of practical interest. For instance, cyclic movements of the ground surface may indicate significant shrink/swell phenomena in expansive soils, bradyseism, or human activity such as injection of gas into a reservoir (Kim et al., 2010; Calabro et al., 2010). Dormant landslides may also show periodic variations of velocity induced by the seasonal fluctuation of the water table, and a sudden change in behavior might indicate a change in the stability conditions.

A convenient way to evaluate the periodicity of a time series is to compute its power spectral density P (Priestley, 1981). The power spectrum is generated by the basic FFT analysis and provides a representation of the magnitude of
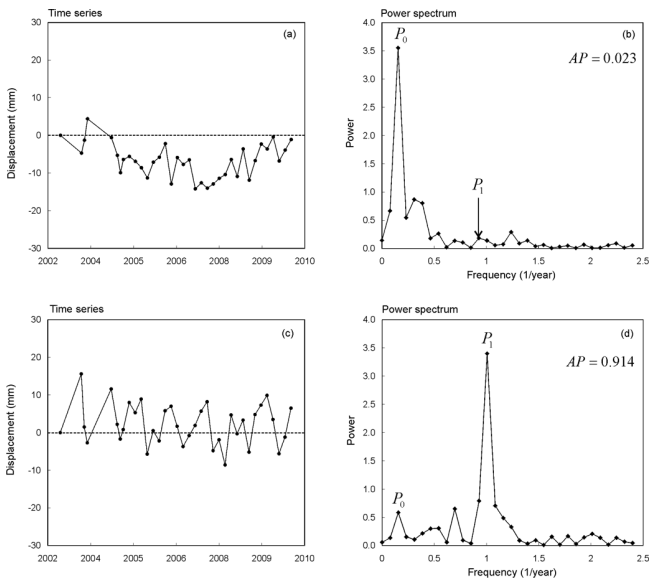
Fig. 4. Comparison of two sample time series characterized by different annual fluctuations (**a** = non-periodic series; **c** = periodic series). Spectral power of the non-periodic series (**b**) exhibits a peak P_0 at the fundamental frequency $f < 0.5$, while periodic series clearly show a spectral peak P_1 at the frequency $f \approx 1\,\mathrm{yr}^{-1}$ (**d**). The index of annual periodicity (AP) is computed by Eq. (6).

the various frequency components (f) of the series. Figure 4 shows the power spectrum $P(f)$ computed for two sample PSI time series, one of which is clearly characterized by periodic fluctuations (Fig. 4c). The x axis covers the frequencies from zero to the Nyquist frequency (half the sampling rate) while the y axis indicates the spectral power. As expected, the periodic series is characterized by a well-defined peak at $f \approx 1\,\mathrm{yr}^{-1}$ (Fig. 4d), while the random series does not show any peak in that frequency range (Fig. 4b). Both the series, however, show a peak in the low-frequency band at $f < 0.5$ which correspond to the fundamental frequency f_0 (that is the frequency associated to the longer waveform fitting the data); when the series follows an half-sine trend (as in Fig. 4a) f_0 is particularly high.

To quantify the annual periodic component, we defined an index of annual periodicity (AP) as the ratio of the power peaks in the two frequency bands $f_0 = 0/0.5\,\mathrm{yr}^{-1}$ (fundamental frequency) and $f_1 = 0.8/1.2\,\mathrm{yr}^{-1}$ (annual frequency):

$$\mathrm{AP} = \begin{cases} 0.5\dfrac{P_1}{P_0} & (\text{if } P_0 \geq P_1) \\[2mm] 1 - 0.5\dfrac{P_0}{P_1} & (\text{if } P_0 < P_1) \end{cases}, \qquad (6)$$

where P_0 and P_1 are the spectral peaks in the two frequency bands (Fig. 4b–d). The index AP ranges from 0 (no annual periodicity) to 1 (very strong annual periodicity). In the example of Fig. 4, AP is 0.02 for the random series and 0.91
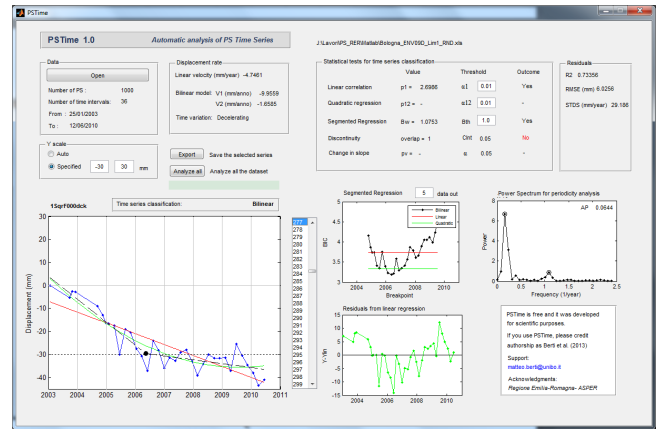
Fig. 5. Graphical user interface of the PS-Time application. The application is freely available at http://www.bigea.unibo.it/it/ricerca/pstime.

for the periodic series. Periodicities other than annual are not captured by AP.

2.5 Graphical user interface

The classification method is integrated into a graphical user interface called PS-Time (Fig. 5). PS-Time is written in Matlab 7.11 and it is freely available as a standalone application that can run on Windows and Unix systems without requiring Matlab or its auxiliary toolboxes (http://www.bigea.unibo.it/it/ricerca/pstime).

The input file is an excel spreadsheet containing the PS data (a sample input file can be found in the web page). PS-Time plots the time series of the selected PS and visualizes the result of the statistical analyses (Fig. 5). Beside the classification of the time series and the analysis of annual periodicity, the program analyzes the residuals of the linear model and computes several descriptive statistical indexes such as the coefficient of determination r^2, the residual mean square error RMSE, and the standard deviation of slope (an index of the scatter of the time series based on the algorithm proposed by Frankel and Dolan (2007) to measure the roughness of natural surfaces).

The button "Analyze all" performs a sequential analysis of all the dataset. The output is an Excel spreadsheet (Table 1) that is ready to be joined to the PS shapefile by the Code field. All the relevant information obtained from the statistical analyses can then be viewed in a geo-referenced GIS software to support the interpretation of PSI data.
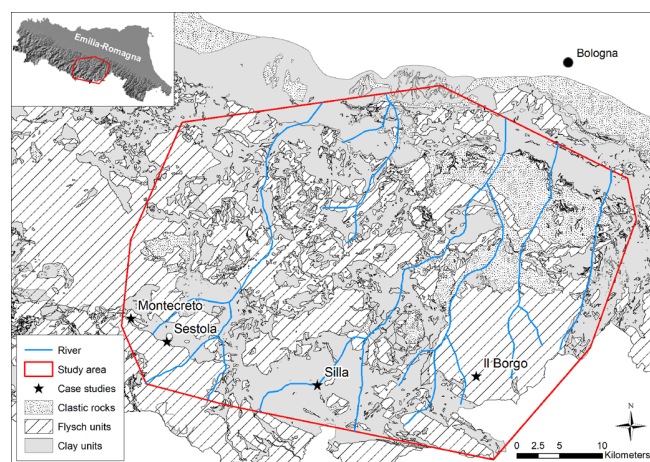
3 Results

3.1 Test area and sample dataset

PS-Time has been calibrated and tested using a PSI dataset covering about $2000\,\mathrm{km}^2$ of the northern Apennines of Italy

Table 1. Output table provided by PS-Time.

Field	Description
Code	PS code used to join the output table to a georeferenced shapefile
VLin	Mean velocity by linear regression (mm yr^{-1})
R2	Coefficient of determination of the linear regression
RMSE	Root mean squared error of the linear regression (mm).
STDS	Standard deviation of slope (mm yr^{-1}) (Frankel and Dolan, 2007)
AP	Index of annual periodicity computed by Eq. (6)
P1	F statistic for the significance of the linear regression (to be compared with the selected level of significance α_1)
P2	F statistic for the significance of the quadratic regression (not used in the classification procedure)
P12	F statistic for the significance of a quadratic term added to a linear regression (to be compared with the selected level of significance α_{12})
BL	Result of the bilinear regression analysis: $0 =$ the bilinear model does not provide a better fit to the data than the linear and quadratic models; $1 =$ the bilinear model provides a better fit
BICW	Evidence ratio of the breakpoint B_w computed by Eq. (4)
Type	Time series classification: $0 =$ uncorrelated; $1 =$ linear; $2 =$ quadratic; $3 =$ bilinear; $4 =$ discontinuous with constant velocity; $5 =$ discontinuous with variable velocity.
V1	Mean velocity before the breakpoint (V_1, mm yr^{-1}) computed by bilinear regression for non-linear time series (types 2 to 5)
V2	Mean velocity after the breakpoint (V_2, mm yr^{-1}) computed by bilinear regression for non-linear time series (types 2 to 5)
Break	Breakpoint date (mm/dd/yyy) computed by bilinear regression for non-linear time series (types 2 to 5)
dV	Change in velocity before and after the breakpoint (mm yr^{-1}): $dV = |V_1 - V|_2$
Acc	Sign of the change in velocity: $-1 =$ deceleration; $0 =$ constant velocity; $1 =$ acceleration
Type3	Time series classification with non-linear trends (types 2 to 5) grouped in a single class: $0 =$ uncorrelated; $1 =$ linear; $6 =$ non-linear

Fig. 6. Schematic geological map of the study area.

(Fig. 6). In the area, elevation ranges from 150 m at the Apennines foothills to the north, to about 1700 m to the south. The main valleys are situated SW–NE and slopes are prevalently exposed to NW and SE. Slope are fairly gentle, 13° in average, with values ranging from flat at valley floors to maximum 35° at crests. Average annual rainfall rate is around 1300–1400 mm yr^{-1}. Bedrock is mainly composed of clayey rocks (flysch, clayshales, chaotic complexes) that are

particularly prone to slope instability. In the test area, dormant and active landslide deposits cover about 25 % of the territory. Landslides mainly consists of complex landslides combining earth slides and earth flows. Their rate of movements is generally slow to extremely slow (mm to cm yr^{-1}), in the range of applicability of space borne interferometry based on monthly revisiting times. Land use is dominated by woodland and pastures, with urbanization being limited to some villages, sparse hamlets and a network of secondary roads. In many cases, villages and hamlets are built on top of, or adjacent to, dormant or active landslide deposits. As building generally behave as persistent scatterers, radar interpretation of PSI datasets is potentially very useful for landslide risk management.

The sample dataset is a product of the EPRS-E national project (Extraordinary Plan for Remote Sensing of the Environment) made available by the Geological Office of Emilia-Romagna Region. It derives from Persistent Scatterers Pairs (PSP) interferometry (Costantini et al., 2008) of 36 Envisat descending scenes. It covers the time span January 2003 to June 2010 with an average temporal sampling of 75 days. Due to the unfavorable land use, to the coarse temporal and spatial resolution of C-band Envisat data and to the relatively high coherence threshold adopted for regional scale PSP processing, the dataset contains "only" 63 707 persistent scatterers, which generally correspond to buildings. Average

density is 35 PS km^{-2}, but it varies significantly in relation to land use: from hundreds PS km^{-2} in areas covered by villages to few PS km^{-2} in areas with sparse hamlets only. As the line of sight of Envisat is directed approximately 282° N, persistent scatterers are more frequent on slopes facing SW to NW. Moreover, since slopes are generally less inclined than satellite's look angle (23.13°), layover or shadowing problems are not relevant.

3.2 Calibration of the statistical thresholds

Before applying the automatic classification procedure, suitable levels of significance must be set (see Sect. 2.2). To this purpose three of the authors performed an expert-based classification of 1000 PS randomly selected within the study area. The results were then compared and discussed to reach a shared classification. In general we found good agreement between the subjective assessment of uncorrelated (type = 0) and linear (type = 1) time series, while it was more difficult to agree on the quadratic (type = 2), bilinear (type = 3) and discontinuous (type = 4 and 5) trends. We then decided to group all the "non-linear" time series (types 2 to 5) into a single class and to restrict the calibration analysis on the statistical thresholds α_1, α_{12}, and B_{th}. These are the significance levels used to discriminate between uncorrelated, linear, and non-linear trends in our automatic procedure (tests A, B, C; Fig. 2).

The optimal values of α_1, α_{12}, and B_{th} were selected using the ROC curve method [Green and Swets, 1966]. The three statistical thresholds were varied in a wide range (α_1, $\alpha_{12} = 1 \times 10^{-5}/0.4$, 57 log-spaced values; $B_{th} = 1.0/1.5$, 11 equally-spaced values) and, for each combination, the performance of the model was evaluated by comparing the automatic with the expert classification.

The results of the analysis are shown Fig. 7. Each point represents the capability of the model to predict a certain type of time series (for instance linear) for a given combination of the statistical thresholds. The more distant a point is from the 1 : 1 line (which indicates a random prediction) the higher the predictive capability of the model. Therefore, the best combination of α_1, α_{12}, and B_{th} is that providing the more distant points for all the three time series types. A good combination seems to be $\alpha_1 = 0.01$, $\alpha_{12} = 0.01$, and $B_{th} = 1.0$, that provides a prediction accuracy of 84 %, 82 %, and 90 % for the uncorrelated, linear, and non-linear time series, respectively (see the black dots in Fig. 7). As expected (see Sect. 2.2) our calibrated significance levels are lower than those usually adopted (0.01 instead of the conventional 0.05) because data are noisy and we therefore need strong evidence (i.e. a lower level of significance) for the null hypothesis.

3.3 Automated time series classification

Results of PS-Time can be analyzed without considering the spatial location of PS, in order to provide a general analysis
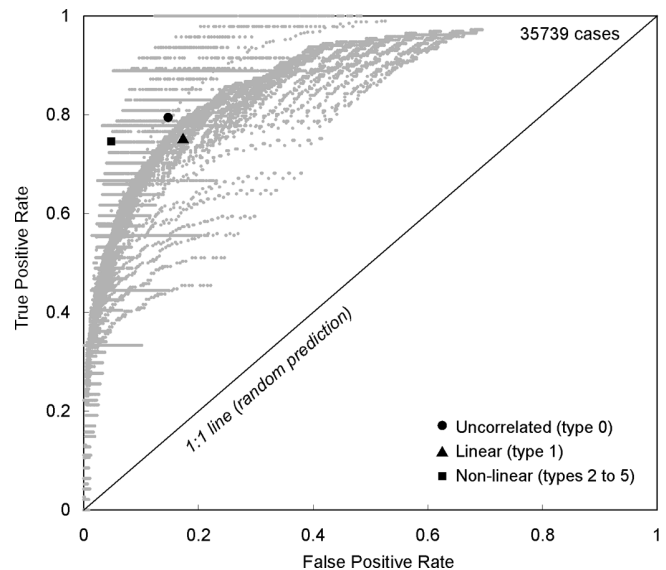

Fig. 7. Results of the ROC curve analysis (Green and Swets, 1966) for the calibration of the statistical thresholds used in PS-Time (α_1, α_{12}, B_{th}). Each point indicates the accuracy of the automatic classification obtained by a given combination of the statistical thresholds with respect an expert-based classification. Black marks indicate the accuracy of the best combination found ($\alpha_1 = 0.01$, $\alpha_{12} = 0.01$, and $B_{th} = 1.0$).

of the time series in the dataset, or they can be displayed on a map to investigate the spatial distribution of target trends with respect to topographic and geologic attributes, such as the known distribution of flat areas, slopes and landslides, or to perform site-specific analyses.

3.3.1 Relative frequency and velocity distribution of classified time series

The pie chart in Fig. 8a shows the percentage distribution of the target trends in the study area. The majority of the time series is classified as "uncorrelated" (59 %) or "linear" (33 %). Non-linear trends (type 2 to 5) account for the 8 % only and mostly consist of bilinear functions. It seems reasonable that in a large area most of the PS are stable or characterized by slow movements without significant variation of velocity, and that non-linear displacements are a small minority. The frequency distributions of the mean displacement rate of the different target trends further support the correctness of the analysis (Fig. 8b). The velocity distribution of uncorrelated time series is centered on zero and nearly all the PS have a velocity between +2 and −2 mm yr^{-1}. Interestingly, this is the velocity threshold typically used to cutoff significant ground movements in practical applications (e.g. Catani et al., 2012). Linear time series show a bimodal distribution with a dominant peak well below zero (−1.5 mm yr^{-1}) and a secondary peak around +1.5 mm yr^{-1}. The distribution is skewed to the left and it
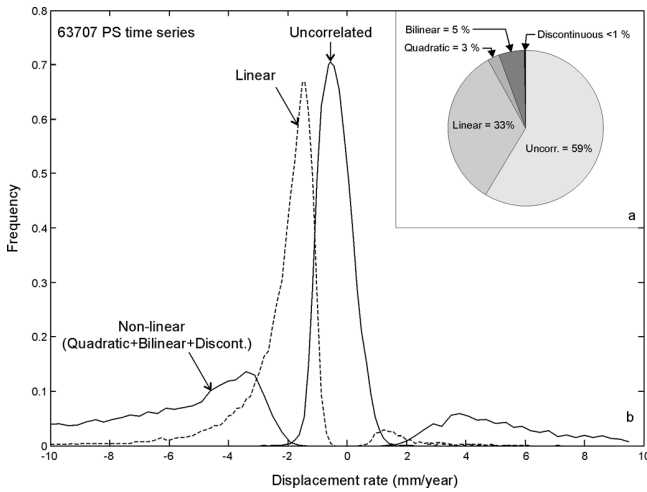
Fig. 8. (a) pie chart showing the relative frequency of the six target trends in the test dataset (type 4 and 5 are not distinguished because of the low percentage); **(b)** frequency distributions of the mean velocity for the different target trends ("non-linear" trends includes types 2 to 5).
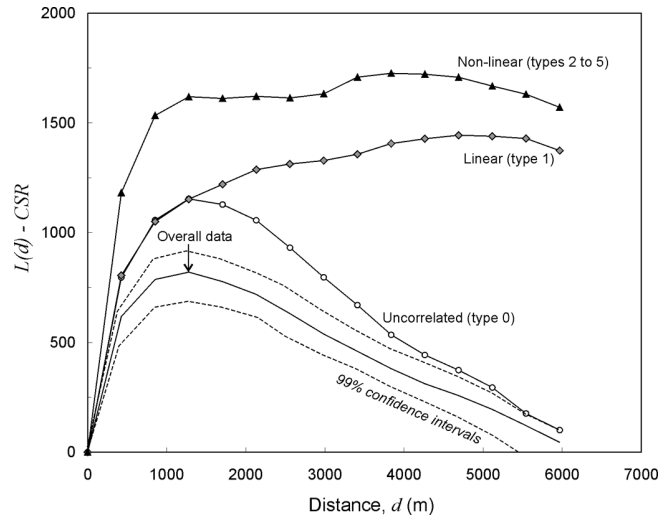

Fig. 9. Cluster analysis of the classified PS. The chart shows the spatial clustering of uncorrelated, linear, and non-linear PS (marked curves) with respect the overall distribution of unclassified PS (unmarked curve). Dashed lines indicate the expected distribution of the classified PS (at 99 % confidence interval) in the hypothesis of a random dispersion within the parent dataset.
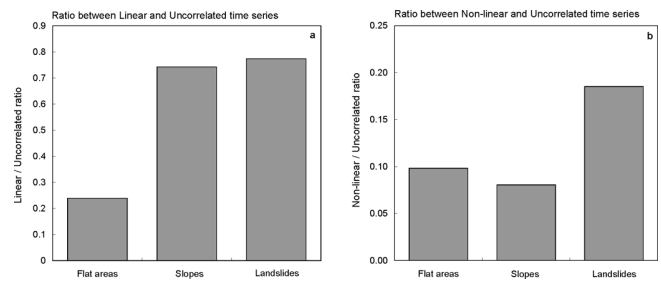

Fig. 10. Relative frequency of linear **(a)** and non-linear **(b)** time series with respect to uncorrelated time series in the three morphological units mapped in the study area.

is clearly separated from that of the uncorrelated PS. Non-linear time series are even more separated and remarkably skewed toward higher displacement rates (both positive or negative). Such a clear distinction between the three frequency distributions suggests that different physical processes are controlling the displacements of uncorrelated, linear, and non-linear PS. The latter, in particular, should be of particular interest since they highlight a radical change of behavior during the monitoring period.

3.3.2 Spatial clustering

A simple way to establish the significance of the method is to see whether the classified PS are clustered or randomly distributed over space. Spatial clustering of the target trends would suggest the existence of a common process influencing the temporal behavior of a group of PS, such as a landslide or local subsidence, while a random distribution would indicate that time series classification not add any significant spatial information.

Most of the methods for cluster analysis compare the pattern of the data to that produced by a homogeneous Poisson process as shown in Haining (2003). In the case of PS, however, data are inherently clustered since the reflecting elements (building, pylons, outcrops) are usually grouped in space (Lu et al., 2012). Therefore, to evaluate if classified PS are spatially aggregated, we have to see if they are more clustered than the parent distribution.

The analysis was performed using the univariate Ripley's K function (Dixon, 2002) and results are shown in Fig. 9. Each curve represents the difference between the "variance stabilized" Ripley's K function (L) and the value expected

for a complete spatial randomness distribution (CSR). The difference L-CSR is plotted against the distance d, which is a scale parameter indicating the size of the cluster: the more the curve is away from the x axis (random distribution) the more clustered are the data. As can be seen, all the classified PS (uncorrelated, linear, non-linear curves) exhibit a strong pattern of spatial clustering and their degree of aggregation is higher than that computed for the parent unclassified PS (overall data curve). Moreover, classified PS fall outside the 99 % confidence intervals of a random distribution (computed by performing 1000 Montecarlo simulations in which the target trends were randomly distributed within the overall clustered domain) thus indicating that the observed differences are statistically significant.

On the other hand, spatial clustering can be clearly recognized on the map. Uncorrelated PS (type 0) are generally concentrated in flat areas such as fluvial terraces and
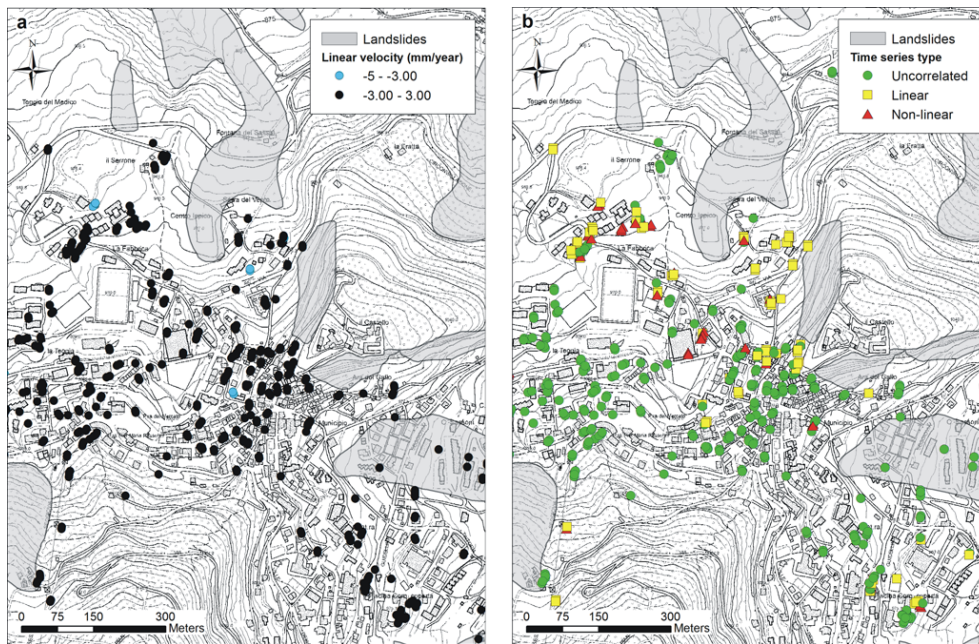
Fig. 11. Sample application of PS-Time to the village of Sestola (Modena province, northern Apennines of Italy). **(a)** mean velocity obtained by linear regression; **(b)** time series classification (non-linear class includes types 2 to 5).

valley bottoms, and along stable watershed divides; linear PS (type 1) are mainly located on slopes (both inside or outside mapped landslides) or near the edge of scarps or steep slopes; non-linear PS (types 2 to 5) typically fall inside landslide deposits or in the surrounding areas. The histograms in Fig. 10 illustrate this general tendency showing that the relative percentage of linear and non-linear PS (with respect uncorrelated PS) increases from flat areas to slopes to landslides. Of course, the spatial distribution of classified PS is more complex when analyzed at the local scale. Ancient dormant landslides, for instance, may show uncorrelated time series (type 0) that indicate the absence of detectable movements, while non-linear PS can be found in flat areas or outside the landslides as a consequence of deformation processes not related to slope instability such as ground subsidence, soil swelling, or structural deformations of buildings. Examples site-specific distributions are discussed in the next section.

4 Discussion

4.1 Enhanced radar interpretation of slope movements

The main strength of the method is to enhance the interpretation of PS data. Different temporal trends likely correspond to different deformation processes, and their spatial distribution can greatly improve our understanding. A first example is given in Fig. 11. The maps show the village of Sestola, a popular tourist center located about 70 km to the south of Modena. The village is surrounded by several landslide bodies, principally dormant earthflows, and threatened by
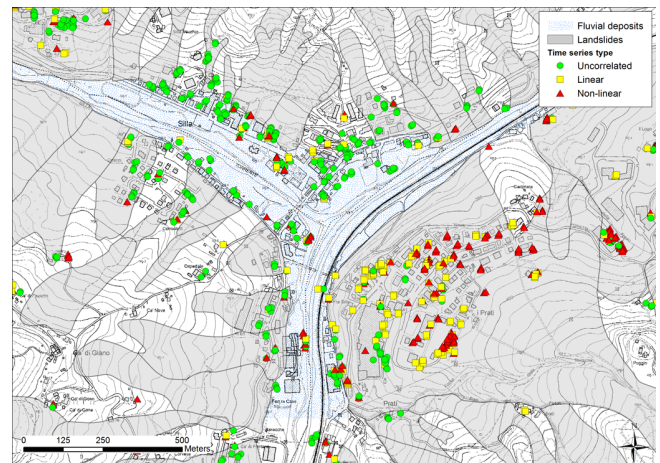

Fig. 12. Classification of PSI time series in the area of Silla (Bologna province, northern Apennines of Italy).

rockfalls from the steep slopes to the south. The vast majority of the 389 PS identified in the area show a very low mean velocity (from -3.0 to $3.0\,\mathrm{mm\,yr^{-1}}$; Fig. 11a) which lead to consider the area as uniformly stable. Time series analysis, however, provides a more accurate picture of the stability conditions. Although most of the PS are characterized by uncorrelated time series (type 0, stable points) several significant clusters of linear (type 1) and non-linear (types 2 to 5) PS appear in the northern sector of the village (Fig. 11b). More attention must be devoted to these areas in spite of the similarity of the mean displacement rate.
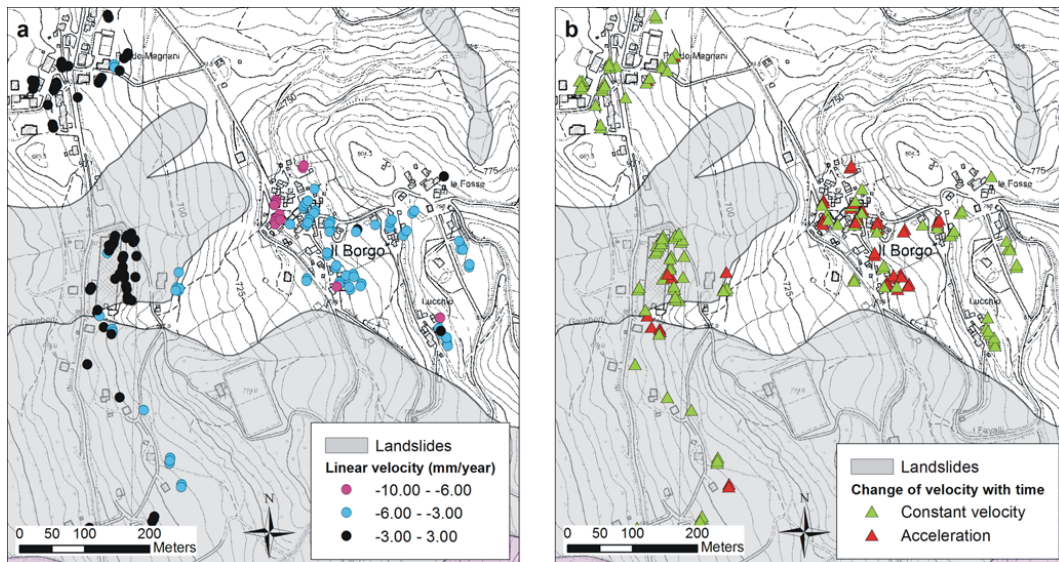
Fig. 13. (a) mean PS velocity in the area of Il Borgo (Bologna province, northern Apennines of Italy); **(b)** PS classification according to the temporal variation of velocity: constant velocity characterizes uncorrelated (type 0) or linear (type 1) time series, acceleration indicates bilinear time series (type 3) with an increasing velocity after the breakpoint.

Another illustrative example is given in Fig. 12. The map shows the confluence between the Reno and the Silla river, about 40 km to the south of Bologna. All the area is deeply affected by earthflows of variable extent and degree of activity. Nearly all the landslides reach the valley bottom, and in recent years several unsafe slopes have been occupied by urban development due to the lack of flat areas. The general distribution of classified PS follows the one previously described. Most of the uncorrelated (stable) PS are located on fluvial terraces or on gently sloping foot slopes, while linear and non-linear PS typically fall inside the landslides. In particular, a large cluster of non-linear PS characterizes the toe of the big earthflow to the east. The extent of the cluster and the fact that most breakpoints occur in the same period (end of 2006) reveal a potentially critical condition. Results are more difficult to interpret when PS with different trends are mixed together without any clear clustering, as in the case of the landslide located in the upper-left corner of Fig. 12. In these cases a close comparison of the time series and a detailed geomorphological analysis must be performed to judge the significance of the detected differences.

Time series analysis may provide useful information even when a critical areal is already clearly visible by the PS velocity alone. The Borgo village, for example, is located about 50 km to the south of Bologna and it is threatened by two dormant earthflows along the southwestern side (Fig. 13). PS velocities clearly indicate on-going deformations behind the landslide scarps (Fig. 13a), but the time series analysis add the useful information that the displacement rate is everywhere constant (linear trends have constant velocity) or increasing (bilinear trends with $V_2 > V_1$) (Fig. 13b). The lack
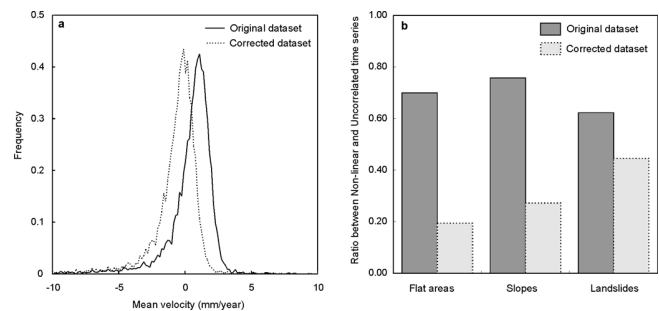

Fig. 14. Application of PS-Time to the biased dataset "Ligonchio". **(a)** frequency distribution of the mean PS velocity of the original (solid line) and corrected (dashed line) dataset; **(b)** relative frequency of non-linear time series in the three morphological units for the biased and corrected dataset.

of decelerating PS and the fact that all the breakpoints fall in the same period (first semester of 2008) are a strong indication of the critical site conditions.

4.2 Influence of dataset's quality

The reliability of the results highly depend on the quality of the dataset. Because of the indirect nature of the radar measurement, and of the many sources of errors involved in the data generation, PSI time series typically show a quite high noise-to-signal ratio. While these errors have a limited impact on the overall linear velocity, they may change the classification outcome.

In general, random errors add spatial noise to the results but do not invalidate the analysis. All the statistical tests, in
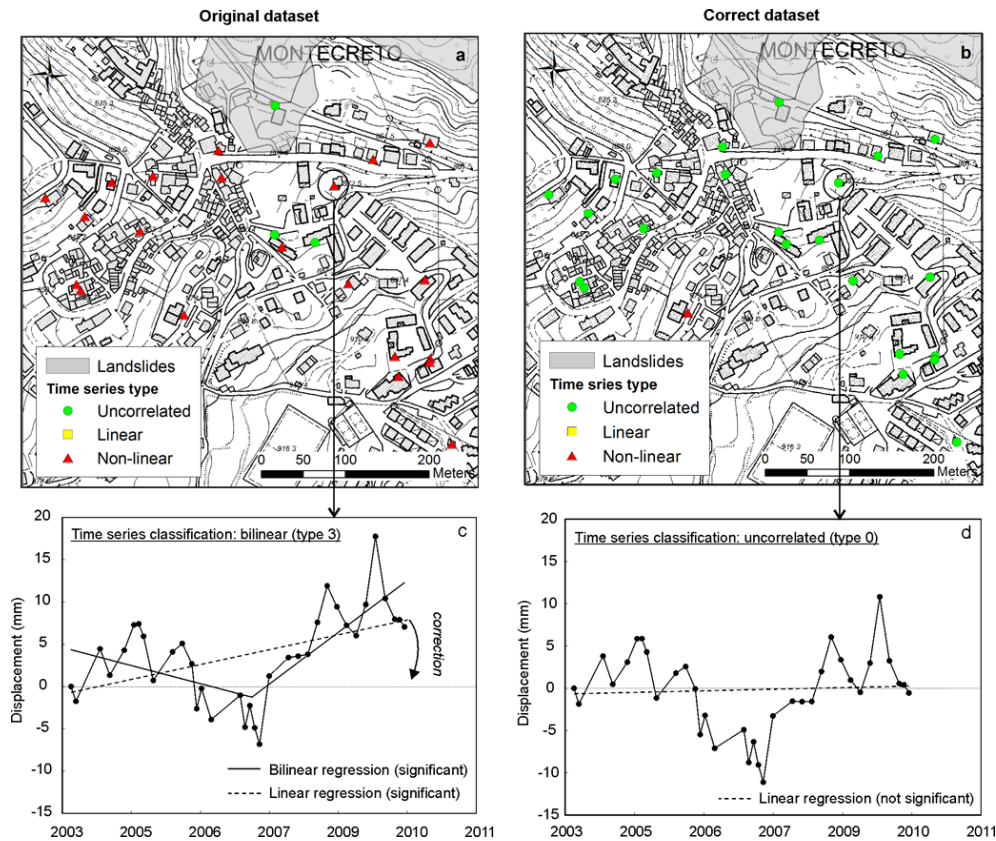
Fig. 15. Comparison of time series classification in the area of Montecreto (Modena province, northern Apennines of Italy) obtained by the original **(a)** and corrected **(b)** dataset. The charts **(c)** and **(d)** show the time series classification of a representative point in the area.

fact, compare a pre-defined regression model (linear, bilinear, quadratic) with a random data distribution and are therefore quite robust in this respect. On the other hand, an erratic drift of several consecutive values at the beginning or at the end of the time series might lead to classify a time series as "bilinear" while it is actually "linear" or "uncorrelated". This problem is quite common in our datasets, and is particularly relevant for slow-moving PS, because random errors have a detrimental effect when the displacement values fluctuate around zero. For this reason a specific function to exclude initial and final data from the time series has been implemented in PS-Time.

A more subtle problem occurs when PSI datasets are affected by a systematic error. For instance, a bias in the displacement values will cumulate over time and will not only give an erroneous value of the average velocity, but it will also add a drift to the time series that might lead to a misleading classification. We have experienced this problem while testing PS-Time using another dataset of EPRS-E national project. Specifically, we analyzed 2000 km^2 of the dataset "Ligonchio" (PSP-IFSAR, December 2003 to July 2010, 35 Envisat ascending scenes, 8737 PS points) which is adjacent to the study area. The entire dataset is affected by a systematic drift of displacement in time, as evidenced by

the shift of the mean velocity distribution toward the positive values (Fig. 14a, solid line). Such a steady movement affects slopes, valley floors and plain areas, and it is clearly not realistic. If this dataset is processed without any correction, the spatial distribution of target trends with respect to flat areas, slopes and mapped landslides is not as expected, since we see no difference in the relative abundance of non-linear time series between the different morphological units (Fig. 14b). However, when the dataset is corrected by applying a velocity offset of -1.15 mm yr^{-1} (in order to adjust the frequency peak to zero; see the dashed line in Fig. 14a), the analysis provides the expected results and a clear clustering of non-linear trends appears within mapped landslides (Fig. 14b). The applied correction changes the classification of 4932 time series over 8737 (56 %) indicating that even a small bias of few mm yr^{-1} may have a deep impact on the results.

To further highlight the problem, consider the example in Fig. 15. The maps show the slope of Montecreto, which is classified by existing landslide inventory maps as a potentially unstable slope. Time series classification based on the original dataset shows 24 time series as bilinear (type $= 3$) and only 3 as uncorrelated (type $= 0$) (Fig. 15a). Moreover, all the bilinear PS are stable until first semester of 2007 and

then start moving at average velocities of 6 mm yr^{-1} (see the example in Fig. 15c). This might induce one to speculate that slope processes are progressing quite rapidly at present and that some cause of reactivation affected the entire slope in 2007. However, time series classification based on the unbiased dataset provides a different, and possibly more realistic, picture. Among the 27 PS only 1 is now classified as "bilinear" and 26 become "uncorrelated" (Fig. 15b). The mean velocity is close to zero for almost all PS, which is consistent to the fact that most of the buildings show no damage and there are no evidence of accelerated slope movements. Still a break in the time series is in 2007 (Fig. 15d) but the velocity after the break is now less than 1 mm yr^{-1}.

5   Conclusions

The new approach for the automatic classification of the Permanent Scatterers time series allows to enhance the radar interpretation of slope movements, providing a better understanding of the deformation phenomena than that based on the conventional analysis of mean velocities alone. The statistical algorithms adopted in the analysis use standard statistical technique to determine whether a measured time series differs significantly from six pre-defined trends recognized by expert visual inspection of 1000 time series. The identified target trends (uncorrelated, linear, quadratic, bilinear, discontinuous with constant velocity, discontinuous with variable velocity) describe different styles of ground deformation and likely indicates the response to different deformation processes.

The application in a study area of the northern Apennines of Italy shows the potential of the method. PS with similar trends are spatially clustered and fairly distributed within the main morphological units, with most of the uncorrelated time series (stable PS) located on the fluvial terraces and in the flat areas, linear PS on slopes, and non-linear PS on landslides. At the local scale, the time series analysis has proven to be an effective integration of the conventional velocity analysis allowing to distinguish between areas characterised by different temporal evolution (constant velocity, acceleration, deceleration, sudden changes of the deformation rate). The test application also shows that the reliability of the results highly depend on the quality of the dataset, and that even a small bias in the data may provide misleading classification of the time series. Therefore, it is important to correct a biased dataset for any systematic error.

Although the method was developed and tested to investigate slope stability, it should also be useful for the analysis of other ground deformation processes such as subsidence, swelling/shrinkage of soils, or uplift due to deep injections. The ever increasing availability of space borne radar data and their increasing quality will make the time series analysis even more powerful.

To promote the use of the method we developed an easy-to-use graphical user interface (called PS-Time) which is freely available as a standalone application (http://www.bigea.unibo.it/it/ricerca/pstime).

References

Berardino, P., Fornaro, G., Lanari, R., and Sansosti, E.: A new algorithm for surface deformation monitoring based on small baseline differential interferograms, IEEE Trans. Geosci. Rem. Sens., 40, 2375–2383, 2002.

Calabro, M. D., Schmidt, D. A., and Roering, J. J.: An examination of seasonal deformation at the Portuguese Bend landslide, southern California, using radar interferometry, J. Geophys. Res., 115, 1–10, doi:10.1029/2009JF001314, 2010.

Catani, F., Canuti, P., and Casagli, N.: The Use of Radar Interferometry in Landslide Monitoring, paper presented at 1st Meeting of Cold Region Landslides Network and 1st Symposium on Landslides in Cold Region, Harbin, China, 2012.

Cigna, F., Del Ventisette, C., Liguori, V., and Casagli, N.: Advanced radar-interpretation of InSAR time series for mapping and characterization of geological processes, Nat. Hazards Earth Syst. Sci., 11, 865–881, doi:10.5194/nhess-11-865-2011, 2011.

Cigna, F., Tapete, D., and Casagli, N.: Semi-automated extraction of Deviation Indexes (DI) from satellite Persistent Scatterers time series: tests on sedimentary volcanism and tectonically-induced motions, Nonlin. Processes Geophys., 19, 643–655, doi:10.5194/npg-19-643-2012, 2012.

Corsini, A., Farina, P., Antonello, G., Barbieri, M., Casagli, N., Coren, F., Guerri, L., Ronchetti, F., Sterzai, P., and Tarchi, D.: Space-borne and ground-based SAR interferometry as tools for landslide hazard management in civil protection, Int. J. Remote Sens., 27, 2351–2369, 2006.

Costantini, M., Falco, S., Malvarosa, F., and Minati, F.: A new method for identification and analysis of persistent scatterers in series of SAR images, paper presented at the International Geosciences Remote Sensing Symposium, Int. Geosci. Remote Sensing Symp. (IGARSS), Boston, USA, 2008.

Davis, J. C.: Statistics and Data Analysis in Geology, John Wiley and Sons, New York, USA, 1986.

Dixon, P. M.: The Ripley's K function, in: Encyclopedia of Environmetrics, Vol. 3, edited by: El-Shaarawi A. H. and Piegorsch, W. W., John Wiley and Sons, Ltd, Chichester, 1796–1803, 2002.

Draper, N. R. and Smith, H.: Applied regression analysis, John Wiley and Sons, New York, USA, 1981.

Farina, P., Casagli, N., and Ferretti, A.: Radar-interpretation of In-SAR measurements for landslide investigations in civil protection practices, in: Proceedings of the 1st North American landslide conference, Vail, 3–7 June 2007, 272–283, 2008.

Farina, P., Casagli, N., and Ferretti, A.: Radar-interpretation of In-SAR measurements for landslide investigations in civil protection practices, paper presented at 1st North American Landslide Conference, Vail, Colorado, USA, 2007.

Ferretti, A., Prati, C., and Rocca, F.: Permanent scatterers in SAR interferometry, IEEE Trans. Geosci. Remote Sens., 39, 8–20, 2001.

Frankel, K. L. and Dolan, J. F.: Characterizing arid-region alluvial fans with airborne laser swath mapping digital topographic data, J. Geophys. Res., 112, F02025, doi:10.1029/2006JF000644, 2007.

Green D. M. and Swets, J. A.: Signal detection theory and psychophysics. New York, Wiley, 455 pp., 1966.

Haining, R.: Spatial data analysis, Cambridge University Press, Cambridge, 2003.

Kim, S. W., Wdowinski, S., Dixon, T., Amelung, F., Won, J. S., and Kim, J. W.: Measurements and predictions of subsidence induced by soil consolidation using permanent scatterer InSAR and hyperbolic model, Geophys. Res. Lett., 37, L05304, doi:10.1029/2009GL041644, 2010.

Lu, P., Casagli, N., Catani, F., and Tofani, V.: Persistent Scatterers Interferometry Hotspot and Cluster Analysis (PSI-HCA) for slow moving landslides detection, Int. J. Remote Sens., 33, 466–489, 2012.

Main, I. G., Leonard, T., Papasouliotis, O., Hatton, C. G., and Meredith, P. G.: One slope or two? Detecting statistically significant breaks of slope in geophysical data with application to fracture scaling relationships, Geophys. Res. Lett., 26, 2801–2804, 1999.

Massonnet, D. and Feigl, K. L.: Radar interferometry and its application to changes in the Earth's surface, Rev. Geophys., 36, 441–500, 1998.

Meisina, C., Zucca, F., Notti, D., Colombo, A., Cucchi, A., Savio, G., Giannico, C., and Bianchi, M.,: Geological Interpretation of PSInSAR Data at Regional Scale, Sensors, 8, 7469–7492, doi:10.3390/s8117469, 2008.

Milone, G. and Scepi, G.: A clustering approach for studying ground deformation trends in Campania Region through the use of PS-InSAR time series analysis, J. Appl. Sci. Res., 11, 610–620, 2011.

Priestley, M. B.: Spectral Analysis and Time Series, Academic Press, New York, USA, 1981.

Schwarz, G.: Estimating the dimension of a model, Ann. Statistics, 6, 461–464, 1978.

Quinn, G. P. and Keough, M. J.: Experimental Design and Data Analysis for Biologists, Cambridge University Press, Cambridge, 2002.

Righini, G., Pancioli, V., and Casagli, N.: Updating landslide inventory maps using Persistent Scatterer Interferometry (PSI), Int. J. Remote Sens., 33, 2068–2096, 2012.

Schwarz, G. E.: Estimating the dimension of a model, Ann. Statistics, 6, 461–464, 1978.

Sen, A. and Srivastava, M.: Regression Analysis: Theory, Methods, and Applications, Springer-Verlag, New York, USA, 1990.

Steven, A. J.: Inference and estimation in a changepoint regression problem, The Statistician, 50, 51–61, 2001.

Wagenmakers, E. J. and Farrell, S.: AIC model selection using Akaike weights, Psychon. Bull. Rev., 11, 192–196, 2004.

Weisberg, S.: Applied Linear Regression, John Wiley & Sons, New York, USA, 1985.

Werner, C., Wegmuller, U., Strozzi, T., and Wiesmann, A.: Interferometric point target analysis for deformation mapping, presented at Geoscience and Remote Sensing Symposium, Int. Geosci. Remote Sensing Symp. (IGARSS), Toulouse, France, 2003.